Numerical Modeling of Scour around Porous Hydraulic Structures: An Evaluation of the Porosity Model

Yalan Song,[1] Hassan Ismail,[2] and Xiaofeng Liu[3]

[1]Department of Civil and Environment Engineering, Pennsylvania State University, University Park, PA 16802, USA; email: yxs275@psu.edu
[2]Department of Civil and Environment Engineering, Pennsylvania State University, University Park, PA 16802, USA; email: hxi33@psu.edu
[3]Department of Civil and Environment Engineering, Institute of Computational and Data Sciences, Pennsylvania State University, University Park, PA 16802, USA; email: xzl123@psu.edu

ABSTRACT

Porous hydraulic structures, such as Large Woody Debris (LWD) and Engineered Log Jams (ELJs), play a very important role in erosion control and habitation conservation in rivers. Previous experimental research has shed some light on the flow and sediment dynamics through and around porous structures. It was found that the scour process is strongly dependent on porosity. Computational models have great value in revealing more details of the processes which are difficult to capture in laboratory experiments. For example, previous computational modeling work has shown that the level of resolution of the complex hydraulic structures in computer models has great effect on the simulated flow dynamics. The less computationally expensive porosity model, instead of resolving all geometric details, can capture the bulk behavior for the flow field, especially in the far field. In the near field where sediment transport is most intensive, the flow result is inaccurate. The way in which this error is translated to the sediment transport results is unknown. This work aims to answer this question. More specifically, the suitability and limitations of using a porosity model in simulating scour around porous hydraulic structures are investigated. To capture the evolution of the sediment bed, an immersed boundary method is implemented. The computational results are compared against flume experiments to evaluate the performance of the porosity model.

INTRODUCTION

Porous structures are essential in river reclamation, including porous groynes, aquatic vegetation patches, Large Woody Debris (LWD) and Engineered Log Jams (ELJs). They can effectively slow down the process of erosion by interrupting flow dynamics to increase bed stability. The physics in these restoration approaches has been investigated by some researchers experimentally and numerically (Chen et al., 2012; Xu and Liu, 2017). Their works focused on the details of turbulent flow and bed response around the porous structures under water. The existence of in-stream porous structures changes flow dynamics by reducing the turbulent kinetic energy (Allen and Smith, 2012), altering local depths (Gippel, 1995) and decreasing total drag coefficient (Gippel et al.,

1992). Correspondingly, the bathymetric response around the porous structure is also altered. For example, the deposition in the wake behind vegetation patches are enhanced because of low velocity and turbulence, which creates favorable conditions for patch expansion (Chen et al., 2012).

In this work, a numerical scour model to simulate bathymetry around a porous structure is developed in which the effect of porosity was represented by a porosity model. An immersed boundary (IB) method was used to capture the bed deformation. The effects of the porosity model on the flow dynamics have been previously studied and shown to perform well in the far-field but fails to capture the flow structure inside and near the porous structure (Xu and Liu, 2017). However, the corresponding effect on the bathymetric response is still unknown. This work analyzed both hydrodynamics and morphodynamics around the porous structure. The suitability and limitations of porosity model in scour evaluation were investigated.

NUMERICAL METHOD

The numerical scour model includes three parts, i.e., hydrodynamic model, morphodynamic model, and porosity model, which are presented separately in this section. The scour model has been implemented in the open source computational physics platform OpenFOAM (OpenFOAM Foundation 2017).

Hydrodynamic Model

The flow is simulated by an immersed boundary method in the framework of the Reynolds-averaged Navier-Stokes (RANS) equations (Egorov and Menter, 2008). The boundary condition of the immersed interface is treated in a Cartesian mesh in which the cells are classified into three categories: IB cells, fluid cells, and solid cells. IB cells are the closest cells to the immersed interface, Γ_{IB}, in the fluid region. The image points (IP) are set on the extended line normal to the immersed interface in the fluid region as shown in Figure 1.

In the immersed boundary method, the shear velocity, u_τ, is calculated using a wall function (Roman et al., 2009) and computed iteratively from:

$$u_\tau^{new} = \frac{u_{tan,IP}}{u^+_{IP,old}(y^+_{IP})} \tag{3}$$

where $u_{tan,IP}$ is the tangential velocity reconstructed on the image point, $y^+ = u_\tau\, y/\nu$, and $u^+_{IP,old}$ is determined by the wall function profile.

The modified velocity on the IB cell center is calculated by the estimated u_τ as:

$$U_{IB} = U_{IP} - \frac{1}{\kappa} u_\tau \log\left(\frac{y_{IP}}{y_{IB}}\right) \tag{4}$$

where κ is the von Karman constant equal to 0.41.

The wall boundary condition is implemented by fixing the value of the modified velocity on the IB cells.

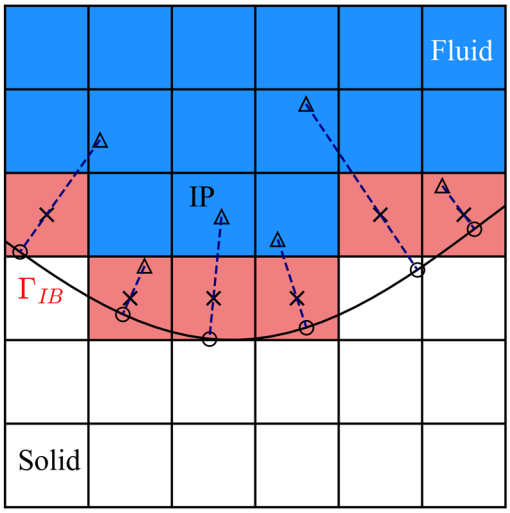

Figure 1. Classification of cells around an immersed interface Γ_{IB}: IB cells (red filled), fluid cells (blue filled), and solid cell (white filled).

Morphodynamic Model

Bed deformation is solved by the Exner equation based on the continuity of sediment as:

$$\frac{\partial z_b}{\partial t} = \frac{1}{1-n}(-\nabla \cdot \mathbf{q}_b) \tag{5}$$

where z_b is the bed elevation, n is the bed porosity, and $\mathbf{q}_b$ is the bedload transport rate.
Only bedload transport is included in this work since all the simulations considered are under the clear-water condition in which there is negligible suspension. The bedload transport rate, $\mathbf{q}_b$, is corrected by the bed slope as:

$$\mathbf{q}_b = q_0 \frac{\boldsymbol{\tau}_b}{|\boldsymbol{\tau}_b|} - C|q_0|\nabla z_b \tag{6}$$

Where C is an empirical constant adopted to control the additional sediment flux due to bed slope (Brørs,1999), $\boldsymbol{\tau}_b$ is the wall shear stress on the bed calculated from hydrodynamic model, and q_0 is bedload transport rate for a flat, horizontal bed calculated by the empirical formula proposed in Engelund and Fredsøe (1976):

$$\frac{q_0}{\sqrt{Rgdd}} = \begin{cases} 18.74(\theta - \theta_c)\left(\theta^{\frac{1}{2}} - 0.7\theta_c^{\frac{1}{2}}\right) & \text{if } \theta > \theta_c \\ 0 & \text{if } \theta > \theta_c \end{cases} \tag{7}$$

where R is the submerged specific gravity (1.65 for quartz), d is the sediment gain size, θ_c is the critical Shields number, and θ is the applied Shields number calculated by $\theta = \frac{|\boldsymbol{\tau}_b|}{\rho g R d}$.

Porosity Model

In the porosity model, the effect of porosity on the flow is represented by adding a resistance force term in the momentum (Eq. 2) using the Darcy-Forchheimer equation:

$$S = -(\nu D + \frac{1}{2}|u|F)u \tag{8}$$

where ν is the kinematic viscosity, u is the flow velocity, the Darcy coefficient, D, and the Forchheimer coefficient, F, are evaluated by:

$$D = \alpha \frac{(1-n)^2}{n^3} \frac{1}{d^{*2}} \tag{9}$$

$$F = 2\beta \frac{1-n}{n^3} \frac{1}{d^*} \tag{10}$$

where α and β are the model constants for calibration, d^* used be to the grain diameter in the original model proposed by van Gent (van Gent, 1996). In this work, it denotes the effective unit size in the porous structure, e.g., the debris size of LWD.

In this work, the calibrated constants are: $\alpha = 200$ and $\beta = 2.0$ (Jansen et al., 2014). Porosity, n, is the ratio of blocked front area to the total front area of the structure.

RESULTS

The scour model for porous structures is utilized to simulate the scour around a nonporous and porous square column. Both columns have a square cross-section in the horizontal plane with an edge length of L = 0.305 m. The structure height is h = 0.61 m. The nonporous structure is an impervious box. The porous structure represents an idealized log crib stacked in a grid pattern with a porosity n of 0.29 as shown in Figure 2. The effective unit size d^* in the porosity model is set as the length of the log 0.305 m.

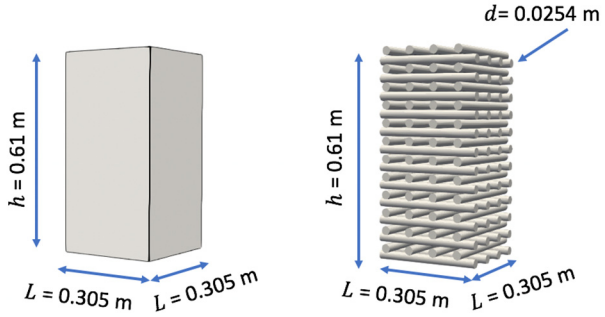

Figure 2. Nonporous and porous structures.

Both structures are sitting at mid-channel and covered to a depth of 0.305 m with sand (d_{sand} = 0.94 mm). The channel has a water depth of 0.305 m and mean velocity of 0.26 m/s. The mesh and simulation setup are shown in Figure 3. Meshes for both cases are refined in the sand zone and

near the structures. The porosity model is applied for porous structure in red square region highlighted in Figure 3(b).

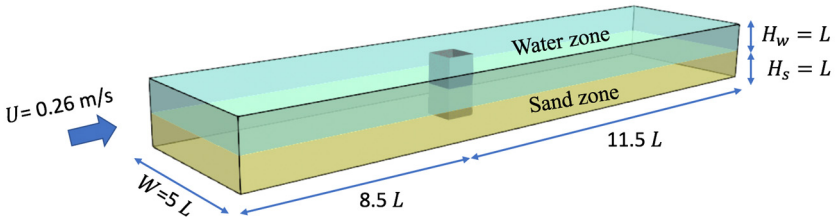

(a) Simulation setup

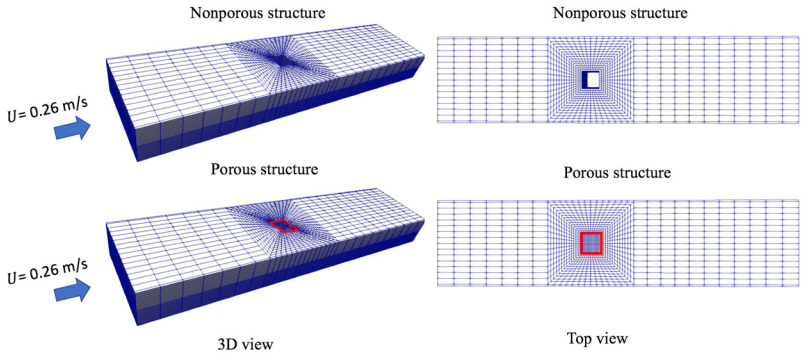

(b) Mesh setup

Figure 3. Setup and mesh for the two simulation cases. Only every fifth cell is shown for clarity.

Figure 4 shows the numerical results of bed elevation for both cases. Both cases have a scour hole (semi-circles) upstream of the structures and deposition in the downstream region. The deepest scour depth occurs at the two upstream corners of the structures. However, laboratory experiments indicated that the deepest scour depth is at the middle of the upstream edge of the structure. As the scour hole upstream deepening, the estimated wall shear stress decreases and becomes smaller than the threshold to trigger sediment transport resulting in mismatch of the simulation and experimental results. Nevertheless, in reality, local erosion and deposition still take place immediately upstream of the structures. Additionally, the deposition bar downstream of the nonporous structure has a higher cross-channel width compared with the porous case because the large-scale vortices with high TKE sweeps the deposited sand from the middle to the sides of channel. However, in the porous case, the flow can pass through the structure and produce a downstream bleed flow in the middle of channel. This bleed flow disturbs and weakens the large-scale vortices in the downstream. As a result, the sand from the upstream deposits and concentrates in the bleed flow zone where the TKE is very low.

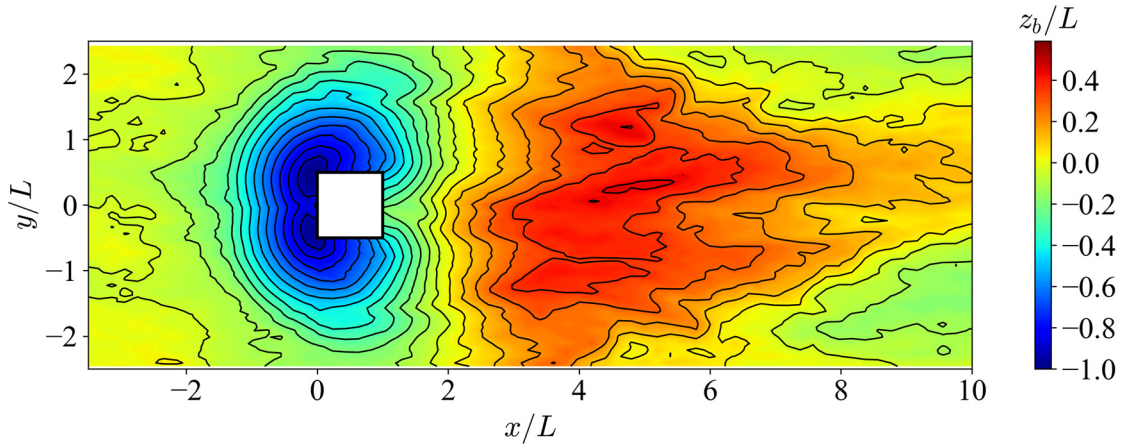

(a) Nonporous structure

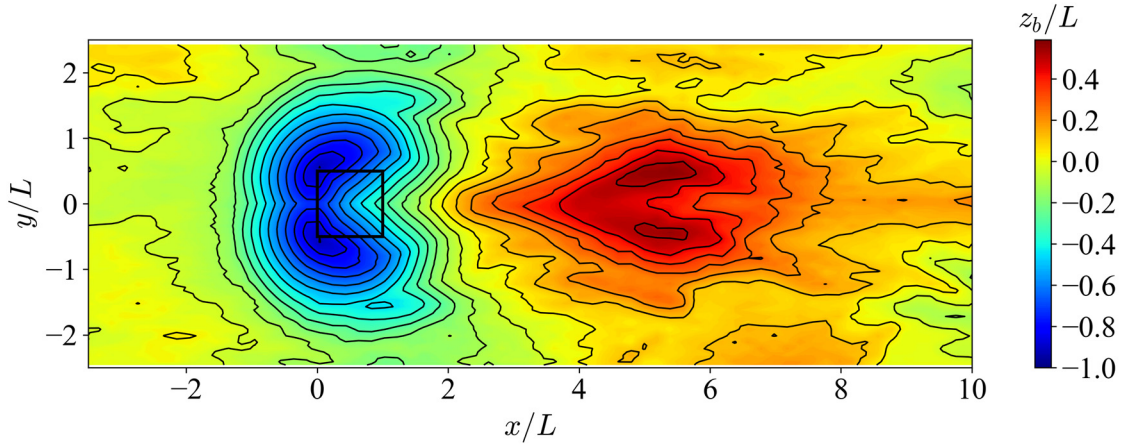

(b) Porous structure

Figure 4. Bed elevation results from the simulations.

Figure 5 shows the comparison of the numerical and experimental results of the bed profile along a streamwise transect along the centerline of the domain. The black line is the simulation result for the nonporous structure. Compared with the result from flume experiment (black triangles), the scour model captured the shape of scour hole well upstream and immediate downstream of the structure, but the computational model over predicted the height of the downstream bar far downstream. The result for the porous structure (blue dash line) has a deeper scour hole upstream and higher deposition downstream compared with the experimental result (blue circles). In addition, the deepest scour in the simulation occurs at the upstream corners of the porous structure where the scour depths are much deeper than expected. The scour hole upstream is related to the horseshoe vortex at the base the structure. In reality, the incoming flow passing through the porous structure will weaken the vortices and convection downward into the scoured hole that would lead to further scouring. However, the porous model is not able to accurately capture the flow structures near and within the porous structure. The effect of the bleed flow on turbulence is not well modeled

by only adding a source term in the momentum equation. Therefore, a modification on the turbulence model of $k-\omega$ is also required for the porous model.

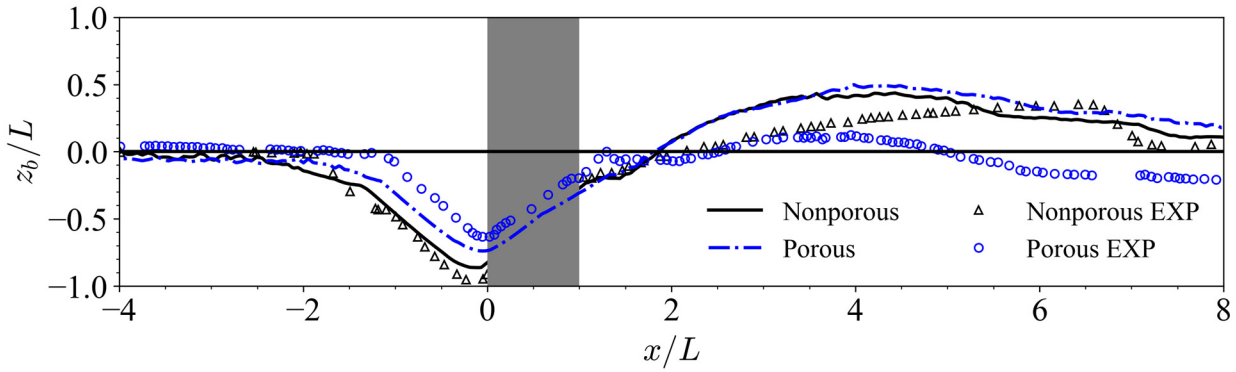

Figure 5. Equilibrium scour profiles along a streamwise transect along the channel center line.

CONCLUSION

In this work, a scour model for porous structures was developed. The effect of porosity is represented by a porosity model by adding a source term in the momentum equation of flow. Two cases were simulated. One is the scour around a nonporous square column and other is the scour around a porous square column. The trend of scour hole was predicted, such as the symmetry of the scour hole along the upstream edge of the structure. However, the porosity model failed to recreate the details of the turbulent flow within the porous structure. As a result, the simulated scour hole is deeper than expected for the porous structure. In future research, a modification on the turbulence equations of $k-\omega$ in porosity model is necessary to properly account for the effect of the porous structure on reducing TKE.

ACKNOWLEDGEMENT

This work is partially supported by a cooperative agreement between Pennsylvania State University and the U.S. Bureau of Reclamation (Award Number R14AC00015 and R17AC00025) and the Strategic Environmental Research and Development Program (SERDP, Award Number W74RDV70063408).

REFERENCES

Allen, J.B. and Smith, D.L., 2012. Characterizing the impact of geometric simplification on large woody debris using CFD. International Journal of hydraulic engineering, 1(2), pp.1-14.

Brørs, B., 1999. Numerical modeling of flow and scour at pipelines. Journal of hydraulic Engineering, 125(5), pp.511-523.

Chen, Z., Ortiz, A., Zong, L. and Nepf, H., 2012. The wake structure behind a porous obstruction and its implications for deposition near a finite patch of emergent vegetation. Water Resources Research, 48(9).

Egorov, Y. and Menter, F., 2008. Development and application of SST-SAS turbulence model in the DESIDER project. In Advances in Hybrid RANS-LES Modelling (pp. 261-270). Springer, Berlin, Heidelberg.

Engelund, F. and Fredsøe, J., 1976. A sediment transport model for straight alluvial channels. Hydrology Research, 7(5), pp.293-306.

Gippel, C.J., 1995. Environmental hydraulics of large woody debris in streams and rivers. Journal of Environmental Engineering, 121(5), pp.388-395.

Gippel, C.J., Finlayson, B.L. and O'Neill, I.C., 1992. The hydraulic basis of snag management. Centre for Environmental Applied Hydrology, Department of Civil and Agricultural Engineering, University of Melbourne.

Greenshields CJ. OpenFoam User Guide, V5. 0. OpenFOAM foundation Ltd. 2017 Jul.

Jensen, B., Jacobsen, N.G. and Christensen, E.D., 2014. Investigations on the porous media equations and resistance coefficients for coastal structures. Coastal Engineering, 84, pp.56-72.

Roman, F., Napoli, E., Milici, B., & Armenio, V. (2009). An improved immersed boundary method for curvilinear grids. Computers & fluids, 38(8), 1510-1527.

Van Gent, M.R.A., 1996. Wave interaction with permeable coastal structures. In International Journal of Rock Mechanics and Mining Sciences and Geomechanics Abstracts (Vol. 6, No. 33, p. 277A).

Xu, Y. and Liu, X., 2017. Effects of Different In-Stream Structure Representations in Computational Fluid Dynamics Models—Taking Engineered Log Jams (ELJ) as an Example. Water, 9(2), p.110.